J Intell Robot Syst (2013) 69:373–387
DOI 10.1007/s10846-012-9719-0

Ground Target Tracking Control System for Unmanned Aerial Vehicles

Tiago Oliveira · Pedro Encarnação

Received: 23 May 2012 / Accepted: 12 July 2012 / Published online: 3 August 2012

Abstract The work here presented contributes to the development of ground target tracking control systems for fixed wing unmanned aerial vehicles (UAVs). The control laws are derived at the kinematic level, relying on a commercial inner loop controller onboard that accepts commands in indicated air speed and bank, and appropriately sets the control surface deflections and thrust in order to follow those references in the presence of unknown wind. Position and velocity of the target on the ground is assumed to be known. The algorithm proposed derives from a path following control law that enables the UAV to converge to a circumference centered at the target and moving with it, thus keeping the UAV in the vicinity of the target even if the target moves at a velocity lower than the UAV stall speed. If the target speed is close to the UAV speed, the control law behaves similar to a controller that tracks a particular point on the circumference centered at the target position. Real flight tests results show the good performance of the control scheme presented.

Keywords Aerial robotics · Target tracking · Moving-path following

T. Oliveira
Science Laboratory,
Portuguese Air Force Academy,
Sintra, 2715-021, Portugal
e-mail: tmoliveira@academiafa.edu.pt

P. Encarnação (✉)
Faculty of Engineering,
Catholic University of Portugal,
Rio de Mouro, 2635-631, Portugal
e-mail: pme@fe.lisboa.ucp.pt

1 Introduction

The Portuguese Air Force Academy (AFA) and the Faculty of Engineering of the University of Porto (FEUP) are developing a Research and Technology Project on Unmanned Air Vehicles with the Portuguese acronym PITVANT, financed by the Portuguese Ministry of National Defense. The main objectives of this seven-year project are the exploration of small platforms and the development of new technologies and new concepts of operation, with an emphasis on the exploration of cooperative control systems for teams of autonomous aerial, marine, and land vehicles. Envisioned mission scenarios encompass aerial surveillance with military applications, search and rescue, forest and coastal patrolling, as well as support/tracking of land or marine vehicles. Although it has received a lot of research interest in the last years, autonomous operation of aerial vehicles is still a challenging task with many open problems, such as trajectory tracking, path following, obstacle detection and avoidance, multi-vehicle

operation, and tracking moving targets, to name just a few. This paper addresses the problem of following a moving target on the ground.

Different strategies have been proposed in the literature for ground target tracking. Lee et al. [1] and Spry et al. [2] designed a controller that switches between two modes according to the relation between the UAV and the target velocities. If both vehicles travel with similar speeds, the UAV performs a sinusoidal trajectory whose baseline is the target trajectory. The amplitude of the sinusoidal trajectory depends on the vehicles' speeds. When the UAV speed is considerably higher than the target speed, the controller switches to a loiter mode setting several waypoints around the target that the UAV should cross.

Dobrokhodov et al. [3] proposed a vision based target tracking system using a guidance based algorithm for tracking a moving target, simultaneously estimating its GPS coordinates. The control objective is to keep the aircraft within a certain range of the target and align the aircraft velocity vector with the perpendicular to the direction of the line that connects the UAV center of mass with the target (perpendicular to the line of sight vector, so the UAV performs a loiter centered at the target). The method was developed considering a static target, and applied without modification for moving targets. By reformulating the control objective presented in [3], Li et al. [4] formally extended the method for moving targets. The guidance law derived is asymptotically stable and thus steady state errors are bounded [4].

In [5] a Lyapunov guidance vector field strategy is used. A vector field with a stable limit circle centered at the target position is determined. From it, a scaled Lyapunov guidance vector is computed and added to the target velocity, if known, to provide a heading command to the UAV. However, this may lead to an oscillating behaviour when the target speed is similar to the UAV.

Trajectory tracking (where a vehicle should follow a given trajectory with time constraints) and path following (where there are no time constraints and the vehicle can thus move with constant speed) control laws for wheeled mobile vehicles have been proposed in a series of groundbreaking papers by Samson et al. [6–8]. More recently, trajectory tracking considering a kinematic model with input constraints was proposed by Ren et al. [9]. For path following, an error space based on the Serret–Frenet frame associated to the path is generally used. The same circle of ideas led to the development of trajectory tracking and path following systems for marine vehicles [10–12] and UAVs [13, 14]. Guidance & control strategies, like trajectory tracking and path following can also be used for target tracking purposes.

Wise and Rysdyk [15] proposed a path following based method for target tracking. The reference path geometry is determined based on the target current position and heading, as well as on a standoff distance. Deviations from this path produce the course angle error and cross track distance, and a "good helmsman behaviour" guidance law is used to smoothly drive the aircraft towards the desired path.

In [16] the authors proposed a combination of UAV trajectory tracking and path following control laws to track a target on the ground. When the UAV is far from the target or when the target's speed is higher than a given threshold based on the UAV's operating speed, a trajectory tracking control law is used accelerating the UAV towards the target; when the UAV is in the vicinity of the target and the target's speed is lower than a given threshold based on the UAV's stall speed, a path following strategy is used to follow a circumference centered at the target's position, thus requiring the UAV to loiter above the target. A novel path following control law that allows convergence to paths that are moving in time was proposed.

The standard approach with UAV control is to assume that the vehicle has an off-the-shelf inner loop controller that accepts references at kinematic level (angular rates and linear velocities) and generates the UAV control signals necessary to follow those references in the presence of model uncertainty and external disturbances, like wind. Outer loop control laws are thus derived using a kinematic model of the vehicle and provide the references to the inner control loop. The same approach is adopted here.

In this paper, a control method that relies on a path following control strategy to follow a circumference with a fixed radius that moves together with the target is presented, assuming

the UAV airspeed is kept constant by the inner loop controller. Having a constant UAV airspeed contributes to the operational safety and prevents sudden thrust bursts necessary to keep up with the target's ground speed. The method proposed, by design, eliminates the oscillation problems observed in other approaches when the target speed is similar to the UAV [5]. The path following controller extends the classic path following algorithms [6, 11, 12] to the case of paths moving jointly with references on the ground. In contrast with the method proposed in [16], the same control law is used in all operating conditions, disregarding the distance between the UAV and the target, and their relative speeds. If the target speed is close to the UAV speed, the control law behaves similar to a controller that tracks a particular point on the circumference centered at the target position. When the ground target moves slower than the UAV, the UAV is required to loiter above it.

The control law is derived using Lyapunov methods assuming that the UAV flies at a constant altitude. The kinematic model for path following is written with respect to the Serret–Frenet frame associated to the reference path [17]. It is considered that the position and velocity of the target is provided to the UAV through an advanced monitoring system (e.g., through satellite monitoring) or, in the case of coordinated missions, by the target itself.

The paper is organized as follows. Section 2 describes the 3D moving-path following algorithm and then applies it to ground target tracking. Section 3 includes a description of the platform and the control architecture used in the flight tests and their results. Finally, Section 4 presents the main conclusions and future work.

2 Ground Target Tracking Control Law

The ground target tracking control law is derived using a path following controller to follow a circumference moving together with the target. The general kinematic model for moving-path following is written with respect to the Serret–Frenet frame associated to the reference path [17]. Consider a local inertial frame $\{I\}$ with its origin at the ground station, x_I axis pointing North, y_I East and z_I Down (this definition is typically referred to as the North–East–Down (NED) with x-North, y-East, and z-Down). Let $\{SF\} = \{\vec{T}, \vec{N}, \vec{B}\}$ be the Serret–Frenet frame associated to the reference path with its x-axis along the tangent to the path, the y-axis normal to the x-axis, always pointing to the right of an observer that moves on the path in the positive direction of the tangent axis, and z-axis pointing down, in accordance to the NED notation [18]. The Serret–Frenet frame can be computed from the parametric equations of the path $p_I(\varphi) = \begin{bmatrix} p_x(\varphi) & p_y(\varphi) & p_z(\varphi) \end{bmatrix}$, where φ is a real parameter and p_I is a path point expressed in the inertial frame, using the well known formulas [17]

$$\vec{T} = \frac{\dot{p}_I(\varphi)}{\|\dot{p}_I(\varphi)\|}; \quad \vec{N} = \frac{\dot{\vec{T}}}{\|\dot{\vec{T}}\|}; \quad \vec{B} = \vec{T} \times \vec{N}. \tag{1}$$

If $\dot{\vec{T}} = 0$ the definition of $\vec{N}$ breaks down. This happens at all points of the path if the path is a straight line. Otherwise, the vanishing of $\dot{\vec{T}}$ is exceptional. In this case there is no basis for calling any particular normal the principal normal. The approach followed was to define $\vec{N}$ as the vector parallel to the horizontal plane, perpendicular to the tangent vector, and pointing to the right of an observer travelling along the positive direction of the path (an alternative approach to avoid the Serret–Frenet frame singularities would be using the parallel transport frame to derive the error space [19]). The distance along the path is denoted by s, and the path curvature κ and the path torsion τ are defined by $\kappa = \|\dot{\vec{T}}\|$ and $\tau = \|\dot{\vec{B}}\|$ [17]. Only paths with constant curvature and torsion are considered on the following derivations (straight lines, circumferences or helices). The $\{I\}$ and $\{SF\}$ frames are depicted in Fig. 1a. Finally, the wind frame $\{W\}$ is located at the vehicle center of mass and has its x_W-axis along the direction of the UAV velocity vector, the y_W-axis parallel to the $x_I - y_I$ plane, normal to x_W, and pointing to the right of an observer that moves in the same direction of the aircraft, and z_W-axis orthogonal to the previous two. From this definition, ${}^W v_W$, the linear velocity of $\{W\}$ relative to $\{I\}$ and expressed

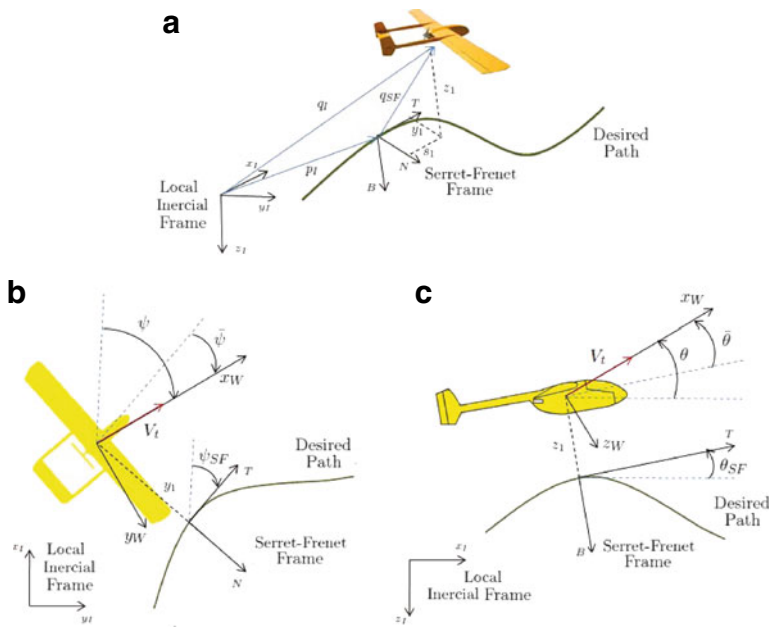

Fig. 1 Path following relevant variables. **a** Error space frames. **b** Lateral dynamics. **c** Longitudinal dynamics

in $\{W\}$, is given by ${}^{W}v_W = \begin{bmatrix} V_t & 0 & 0 \end{bmatrix}^T$, where V_t denotes the aircraft ground speed.

Let ψ be the angle between the projection of the UAV velocity vector onto the $x_I - y_I$ plane and North, and θ the angle between the UAV velocity vector and the $x_I - y_I$ plane, positive if the aircraft is above the ground. Note that these are not regular yaw and pitch angles since they are the angles between the wind frame and the inertial frame instead of the angles between a body frame attached to the UAV and the inertial frame. Figure 1b and c shows the error space for path following.

The aircraft center of mass coordinates are denoted by $q_I = \begin{bmatrix} x & y & z \end{bmatrix}^T$ when expressed in the inertial frame $\{I\}$ and by $q_{sf} = \begin{bmatrix} s_1 & y_1 & z_1 \end{bmatrix}^T$ when expressed in the Serret–Frenet frame. For path following applications, the $\{SF\}$ frame is placed at the closest to the vehicle point on the path, thus yielding s_1 equal to zero. Note however that it is assumed that the path is moving in time at a fixed altitude, thus each path point is moving with a velocity $v_r = \begin{bmatrix} v_x & v_y & 0 \end{bmatrix}^T$ relative to $\{I\}$ and expressed in $\{I\}$. Let ϕ_{sf}, θ_{sf} and ψ_{sf} be the roll, pitch and yaw angles of the $\{SF\}$ frame with respect to $\{I\}$. The angular displacements between the wind frame and the Serret–Frenet frame are $\bar{\phi} = -\phi_{sf}$, $\bar{\psi} = \psi - \psi_{sf}$ and $\bar{\theta} = \theta - \theta_{sf}$ (see Fig. 1). According to the Serret–Frenet formulas [17], the angular velocity of the Serret–Frenet frame with respect to the inertial frame, written in the $\{SF\}$ frame, is given by ${}^{SF}\omega_{SF} = \begin{bmatrix} \tau\dot{s} & 0 & \kappa\dot{s} \end{bmatrix}^T$.

The linear velocity of $\{W\}$ relative to $\{I\}$ and expressed in $\{I\}$ is given by

$$ {}^{I}v_W = \begin{bmatrix} \dot{x} & \dot{y} & \dot{z} \end{bmatrix}^T = {}^{I}R_W(\theta, \psi)\ {}^{W}v_W, \tag{2} $$

where ${}^{I}R_W(\theta, \psi)$ is the rotation matrix from $\{W\}$ to $\{I\}$ [20]

$$ {}^{I}R_W(\theta, \psi) = \begin{bmatrix} \cos\psi\cos\theta & -\sin\psi & \cos\psi\sin\theta \\ \sin\psi\cos\theta & \cos\psi & \sin\psi\sin\theta \\ -\sin\theta & 0 & \cos\theta \end{bmatrix}, \tag{3} $$

thus,

$$ \begin{aligned} \dot{x} &= V_t \cos\theta\ \cos\psi \\ \dot{y} &= V_t \cos\theta\ \sin\psi \\ \dot{z} &= -V_t \sin\theta. \end{aligned} \tag{4} $$

The angular rates $\dot{\theta}$ and $\dot{\psi}$ are related to the angular velocity of the wind frame with respect to the inertial frame, expressed in the wind frame,

${}^{W}\omega_{W} = \begin{bmatrix} q_w & r_w \end{bmatrix}^{T}$ through the Jacobian operator [20] (note that the wind frame roll angle is, by definition, always equal to zero)

$$\begin{bmatrix} \dot{\theta} \\ \dot{\psi} \end{bmatrix} = \begin{bmatrix} 1 & 0 \\ 0 & \sec\theta \end{bmatrix} \begin{bmatrix} q_w \\ r_w \end{bmatrix}. \tag{5}$$

The position of the UAV in the $\{I\}$ frame can be written as (Fig. 1)

$$q_I = p_I + {}^{I}R_{SF}\left(\phi_{sf}, \theta_{sf}, \psi_{sf}\right) q_{SF} \tag{6}$$

where the rotation matrix ${}^{I}R_{SF}\left(\phi_{sf}, \theta_{sf}, \psi_{sf}\right)$ from $\{SF\}$ to $\{I\}$ is

$${}^{I}R_{SF}\left(\phi_{sf}, \theta_{sf}, \psi_{sf}\right) = \begin{bmatrix} C\psi_{sf}C\theta_{sf} & -S\psi_{sf}C\phi_{sf} + C\psi_{sf}S\theta_{sf}S\phi_{sf} & S\psi_{sf}S\phi_{sf} + C\psi_{sf}S\theta_{sf}C\phi_{sf} \\ S\psi_{sf}C\theta_{sf} & C\psi_{sf}C\phi_{sf} + S\psi_{sf}S\theta_{sf}S\phi_{sf} & -C\psi_{sf}S\phi_{sf} + S\psi_{sf}S\theta_{sf}C\phi_{sf} \\ -S\theta_{sf} & C\theta_{sf}S\phi_{sf} & C\theta_{sf}C\phi_{sf} \end{bmatrix}$$

($S(.)$ and $C(.)$ denote respectively the sine and cosine trigonometric functions).

Differentiating Eq. 6 with respect to time [20] yields

$$\dot{q}_I = \dot{p}_I + {}^{I}R_{SF}\left(\phi_{sf}, \theta_{sf}, \psi_{sf}\right) \begin{bmatrix} \dot{s}_1 \\ \dot{y}_1 \\ \dot{z}_1 \end{bmatrix} + {}^{I}R_{SF}\left(\phi_{sf}, \theta_{sf}, \psi_{sf}\right) S_{kw}\left({}^{SF}\omega_{SF}\right) \begin{bmatrix} s_1 \\ y_1 \\ z_1 \end{bmatrix}, \tag{7}$$

where $S_{kw}(.)$ is a skew-symmetric matrix that satisfies $S_{kw}(a)\, b = a \times b$.

Pre-multiplying by ${}^{SF}R_I\left(\phi_{sf}, \theta_{sf}, \psi_{sf}\right)$ and since $s_1 = \dot{s}_1 = 0$ one obtains

$${}^{SF}R_I\left(\phi_{sf}, \theta_{sf}, \psi_{sf}\right) \dot{q}_I = {}^{SF}R_I\left(\phi_{sf}, \theta_{sf}, \psi_{sf}\right) \dot{p}_I + \begin{bmatrix} 0 \\ \dot{y}_1 \\ \dot{z}_1 \end{bmatrix} + \begin{bmatrix} -\kappa\dot{s}\, y_1 \\ -\tau\dot{s}\, z_1 \\ \tau\dot{s}\, y_1 \end{bmatrix}. \tag{8}$$

Using the properties of the rotation matrices,

$${}^{SF}R_I\left(\phi_{sf}, \theta_{sf}, \psi_{sf}\right) = {}^{SF}R_W\left(\bar{\phi}, \bar{\theta}, \bar{\psi}\right)^{W} R_I\left(\theta, \psi\right) \tag{9}$$

and thus

$${}^{SF}R_I\left(\phi_{sf}, \theta_{sf}, \psi_{sf}\right) \dot{q}_I = {}^{SF}R_W\left(\bar{\phi}, \bar{\theta}, \bar{\psi}\right)^{W} v_W. \tag{10}$$

The linear velocity ${}^{SF}R_I\left(\phi_{sf}, \theta_{sf}, \psi_{sf}\right) \dot{p}_I$ of a point on the path relative to $\{I\}$ and expressed in $\{SF\}$ is the sum of the linear velocity of the point relative to $\{SF\}$ with the velocity of the Serret–Frenet frame relative to $\{I\}$, both expressed in $\{SF\}$, i.e.

$${}^{SF}R_I\left(\phi_{sf}, \theta_{sf}, \psi_{sf}\right) \dot{p}_I = \begin{bmatrix} \dot{s} & 0 & 0 \end{bmatrix}^{T} + {}^{SF}R_I\left(\phi_{sf}, \theta_{sf}, \psi_{sf}\right) \begin{bmatrix} v_x \\ v_y \\ 0 \end{bmatrix}. \tag{11}$$

Therefore, Eq. 8 can be rewritten as

$${}^{SF}R_W\left(\bar{\phi}, \bar{\theta}, \bar{\psi}\right) \begin{bmatrix} V_t \\ 0 \\ 0 \end{bmatrix} = \begin{bmatrix} \dot{s} \\ 0 \\ 0 \end{bmatrix} + {}^{SF}R_I\left(\phi_{sf}, \theta_{sf}, \psi_{sf}\right) \begin{bmatrix} v_x \\ v_y \\ 0 \end{bmatrix} + \begin{bmatrix} 0 \\ \dot{y}_1 \\ \dot{z}_1 \end{bmatrix} + \begin{bmatrix} \kappa\dot{s}\, y_1 \\ -\tau\dot{s}\, z_1 \\ \tau\dot{s}\, y_1 \end{bmatrix} \tag{12}$$

which is equivalent, assuming $1 - \kappa\, y_1 \neq 0$, to

$$\begin{aligned} \dot{s} &= \frac{V_t \cos\bar{\theta}\cos\bar{\psi} - v_x \cos\psi_{sf}\cos\theta_{sf} - v_y \sin\psi_{sf}\cos\theta_{sf}}{1 - \kappa y_1} \\ \dot{y}_1 &= V_t \cos\bar{\theta}\sin\bar{\psi} + \tau\dot{s}z_1 \\ &\quad + v_x\left(\sin\psi_{sf}\cos\phi_{sf} - \cos\psi_{sf}\sin\theta_{sf}\sin\phi_{sf}\right) \\ &\quad - v_y\left(\cos\psi_{sf}\cos\phi_{sf} + \sin\psi_{sf}\sin\theta_{sf}\sin\phi_{sf}\right) \\ \dot{z}_1 &= -V_t \sin\bar{\theta} - \tau\dot{s}y_1 \\ &\quad - v_x\left(\sin\psi_{sf}\sin\phi_{sf} + \cos\psi_{sf}\sin\theta_{sf}\cos\phi_{sf}\right) \\ &\quad + v_y\left(\cos\psi_{sf}\sin\phi_{sf} - \sin\psi_{sf}\sin\theta_{sf}\cos\phi_{sf}\right). \end{aligned} \tag{13}$$

The relative angular velocity between the $\{SF\}$ frame and the wind frame $\{W\}$, expressed in $\{W\}$, is given by

$$^{W}\omega^{r}_{W,SF} = {}^{W}\omega_{W} - {}^{W}\omega_{SF} \tag{14}$$

$$\begin{bmatrix} \bar{p} \\ \bar{q} \\ \bar{r} \end{bmatrix} = \begin{bmatrix} 0 \\ q_w \\ r_w \end{bmatrix} - {}^{W}\omega_{SF} \tag{15}$$

where

$$\begin{aligned} {}^{W}\omega_{SF} &= {}^{W}R_{SF}\left(\bar{\phi},\bar{\theta},\bar{\psi}\right) {}^{SF}\omega_{SF} \\ &= {}^{W}R_{SF}\left(\bar{\phi},\bar{\theta},\bar{\psi}\right) \begin{bmatrix} \tau\dot{s} \\ 0 \\ \kappa\dot{s} \end{bmatrix}. \end{aligned} \tag{16}$$

Using again the Jacobian operator that relates the roll, pitch and yaw angle rates with the angular velocities [20],

$$\begin{bmatrix} \dot{\bar{\phi}} \\ \dot{\bar{\theta}} \\ \dot{\bar{\psi}} \end{bmatrix} = \begin{bmatrix} 1 & \sin\bar{\phi}\tan\bar{\theta} & \cos\bar{\phi}\tan\bar{\theta} \\ 0 & \cos\bar{\phi} & -\sin\bar{\phi} \\ 0 & \dfrac{\sin\bar{\phi}}{\cos\bar{\theta}} & \dfrac{\cos\bar{\phi}}{\cos\bar{\theta}} \end{bmatrix} \begin{bmatrix} \bar{p} \\ \bar{q} \\ \bar{r} \end{bmatrix}. \tag{17}$$

The roll rate equation can be omitted since errors in roll between $\{W\}$ and $\{SF\}$ do not affect convergence to the path (in practice, the vehicle will assume the roll angle that enables it to follow the path).

Solving Eq. 15 with respect to the pitch and yaw angle rates gives

$$\begin{bmatrix} \dot{\bar{\theta}} \\ \dot{\bar{\psi}} \end{bmatrix} = D\left(\bar{\theta},\bar{\psi}\right) + T\left(\bar{\phi},\bar{\theta}\right) \begin{bmatrix} q_w \\ r_w \end{bmatrix} \tag{18}$$

with

$$D\left(\bar{\theta},\bar{\psi}\right) = \begin{bmatrix} \tau\,\dot{s}\,\sin\,\bar{\psi} \\ -\tau\,\dot{s}\,\cos\,\bar{\psi}\,\tan\,\bar{\theta} - \kappa\,\dot{s} \end{bmatrix} \text{and} \tag{19}$$

$$T\left(\bar{\phi},\bar{\theta}\right) = \begin{bmatrix} \cos\bar{\phi} & -\sin\bar{\phi} \\ \dfrac{\sin\bar{\phi}}{\cos\bar{\theta}} & \dfrac{\cos\bar{\phi}}{\cos\bar{\theta}} \end{bmatrix}. \tag{20}$$

Using the feedback linearization law

$$\begin{bmatrix} q_w \\ r_w \end{bmatrix} = T^{-1}\left(\bar{\phi},\bar{\theta}\right)\left(\begin{bmatrix} u_\theta \\ u_\psi \end{bmatrix} - D\left(\bar{\theta},\bar{\psi}\right)\right) \tag{21}$$

one can write

$$\begin{aligned} \ddot{\bar{\theta}} &= u_\theta \\ \ddot{\bar{\psi}} &= u_\psi. \end{aligned} \tag{22}$$

The complete error space for path following purposes is thus

$$\begin{aligned} \dot{s} &= \frac{V_t\cos\bar{\theta}\cos\bar{\psi} - v_x\cos\psi_{sf}\cos\theta_{sf} - v_y\sin\psi_{sf}\cos\theta_{sf}}{1-\kappa y_1} \\ \dot{y}_1 &= V_t\cos\bar{\theta}\sin\bar{\psi} + \tau\dot{s}z_1 \\ &\quad + v_x\left(\sin\psi_{sf}\cos\phi_{sf} - \cos\psi_{sf}\sin\theta_{sf}\sin\phi_{sf}\right) \\ &\quad - v_y\left(\cos\psi_{sf}\cos\phi_{sf} + \sin\psi_{sf}\sin\theta_{sf}\sin\phi_{sf}\right) \\ \dot{z}_1 &= -V_t\,\sin\bar{\theta} - \tau\dot{s}y_1 \\ &\quad - v_x\left(\sin\psi_{sf}\sin\phi_{sf} + \cos\psi_{sf}\sin\theta_{sf}\cos\phi_{sf}\right) \\ &\quad + v_y\left(\cos\psi_{sf}\sin\phi_{sf} - \sin\psi_{sf}\sin\theta_{sf}\cos\phi_{sf}\right) \\ \ddot{\bar{\theta}} &= u_\theta \\ \ddot{\bar{\psi}} &= u_\psi, \end{aligned} \tag{23}$$

assuming $y_1 \neq \frac{1}{\kappa}$ and $|\bar{\theta}| < \pi/2$.

A path following control law should drive the linear distances y_1 and z_1 to zero and orient the UAV such that its velocity vector becomes aligned with the sum of the Serret–Frenet tangent vector and the velocity of the Serret–Frenet frame origin. This three dimensional kinematic model encompasses the classical situation of following paths that are fixed in space [6, 11].

The proposed strategy to track a target on the ground is to follow a circumference with a fixed radius centered at the actual target position, keeping the UAV altitude constant (Fig. 2).

Thus, for this application, $\phi_{sf} = \bar{\phi} = \bar{\theta} = \tau = 0$ and the error space Eq. 23 can be simplified to yield

$$\begin{aligned} \dot{s} &= \frac{V_t\,\cos\bar{\psi} - v_x\,\cos\psi_{sf} - v_y\,\sin\psi_{sf}}{1-\kappa\,y_1} \\ \dot{y}_1 &= V_t\,\sin\bar{\psi} + v_x\,\sin\psi_{sf} - v_y\,\cos\psi_{sf} \\ \ddot{\bar{\psi}} &= u_\psi. \end{aligned} \tag{24}$$

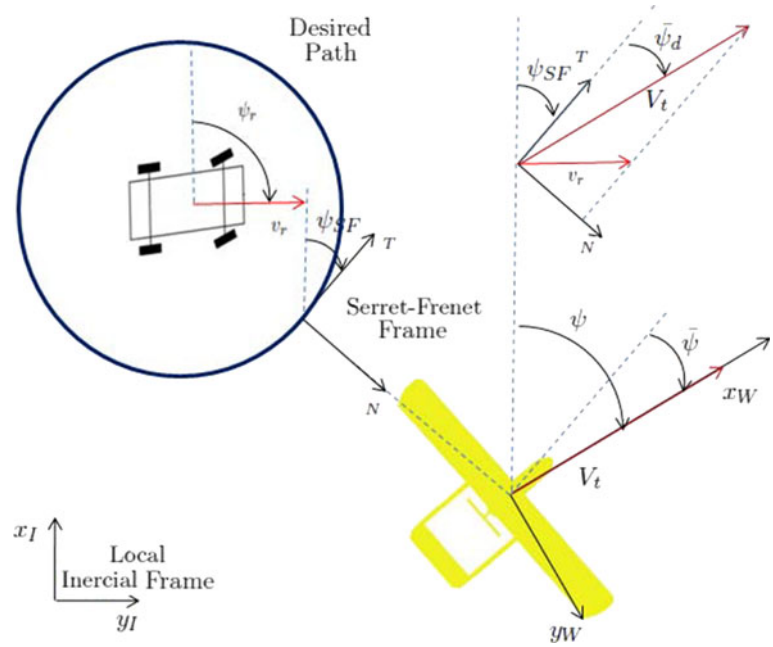

Fig. 2 Moving-path following: relevant variables

The steady state value $\bar{\psi}_d$ for ψ can be computed from Eq. 24 setting $\dot{y}_1 = 0$:

$$\bar{\psi}_d = \arcsin\left(\frac{-v_x \sin\psi_{sf} + v_y \cos\psi_{sf}}{V_t}\right). \tag{25}$$

The numerator of the arcsin argument in Eq. 25 is the target's speed along the normal to the path. Equation 25 is always well defined if the UAV speed V_t is greater than the target speed $\|v_r\|$ and thus the path following problem is well posed. Being the target/path kinematic equations given in terms of the total speed $||v_r||$ and the yaw angle ψ_r by

$$\begin{aligned}\dot{x}_r &= v_x = ||v_r|| \cos\psi_r \\ \dot{y}_r &= v_y = ||v_r|| \sin\psi_r,\end{aligned} \tag{26}$$

and considering the particular case when the UAV speed $||V_t||$ is equal to $||v_r||$, Eq. 25 yields

$$\begin{aligned}\bar{\psi}_d &= \arcsin\left(\frac{-V_t \cos\psi_r \sin\psi_{sf} + V_t \sin\psi_r \cos\psi_{sf}}{V_t}\right) \\ &= \arcsin\left(\sin\left(\psi_r - \psi_{sf}\right)\right).\end{aligned} \tag{27}$$

Thus, in this case, (assuming $|\psi_r - \psi_{sf}| \leq \pi$)

$$\bar{\psi}_d + \psi_{sf} = \psi_r, \quad \psi_r - \psi_{sf} \in \left[-\frac{\pi}{2}, \frac{\pi}{2}\right] \tag{28}$$

$$\bar{\psi}_d + \psi_{sf} = \pi - \psi_r + 2\,\psi_{sf},$$

$$\psi_r - \psi_{sf} \in \left[-\pi, -\frac{\pi}{2}\right[\cup \left]\frac{\pi}{2}, \pi\right[. \tag{29}$$

Figure 3 illustrates this behaviour, considering that the target is heading North.

When the UAV moves at the same speed as the target and it's on the left hand side of it (where Eq. 29 applies), the UAV will keep following the path (compensating for the target's velocity component normal to the $\{SF\}$ frame) converging to the right hand side of the target. Once there, where Eq. 28 applies, the desired orientation will be parallel to the target, thus requiring the UAV to follow a straight line parallel to the target. This avoids an oscillating behaviour when the target speed is similar to the UAV, reported for other approaches [5]. When the target is not moving, the UAV's desired heading is tangent to the circumference (Fig. 4).

In order to avoid situations in which the UAV is required to fly near its stall speed, it is desirable

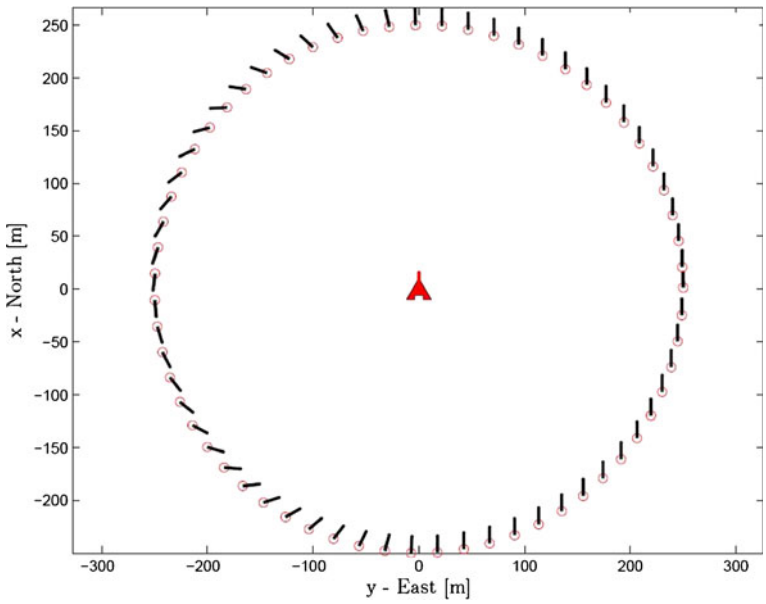

Fig. 3 UAV's desired course when $\frac{v_r}{V_t} = 1$

to keep the vehicle airspeed constant. Commercial autopilots usually accept airspeed references, expressed in the vehicle body frame. The vehicle velocity relative to $\{I\}$ and expressed in the wind frame $\{W\}$, is given by

$$^{W}v_W = {}^{W}R_B\,(\alpha, \beta)\,U_0 + {}^{W}R_I\,(\theta, \psi)^{I}\,v_{\text{wind}} \qquad (30)$$

where ${}^{I}v_{\text{wind}}$ denotes the velocity of the wind relative to $\{I\}$ and written in the body-frame $\{B\}$ and ${}^{W}R_B$ is a rotation matrix parameterized by the vehicle angle of attack α and the sideslip angle β [17]. For the UAVs of the PITVANT project these angles are usually small, and therefore it is reasonable to assume that ${}^{W}R_B = I$. With this

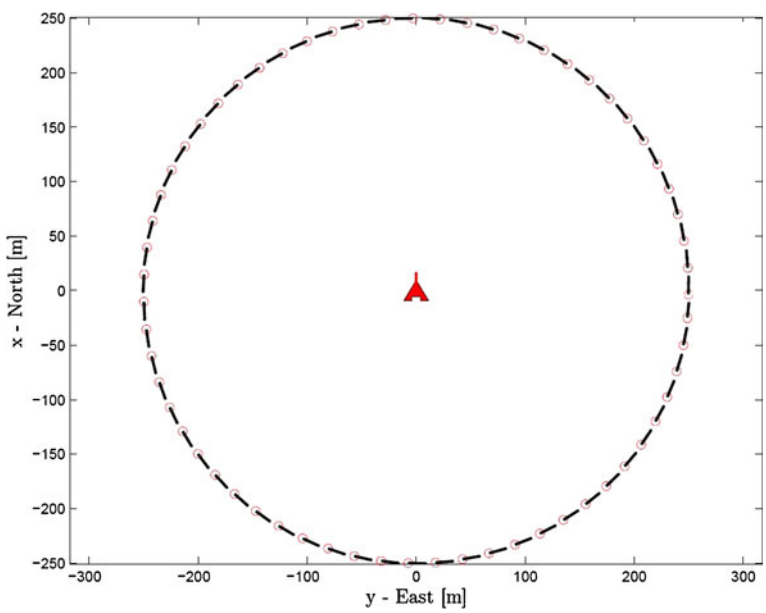

Fig. 4 UAV's desired course when $\frac{v_r}{V_t} = 0$

assumption (and since $\theta = 0$ for planar reference paths), one can write the UAV's ground speed as:

$$V_t = U_0 + W_t, \tag{31}$$

where W_t is the tangential component of the wind pointing in the same direction as the velocity vector of the aircraft, being given by

$$W_t = w_x \cos\psi + w_y \sin\psi. \tag{32}$$

The derivative of $\bar{\psi}_d$ with respect to time, that will be necessary in the sequence, assuming that the autopilot is able to keep U_0 constant is

$$\dot{\bar{\psi}}_d = \frac{\rho}{V_t\sqrt{1-\left(\frac{-v_x \sin\psi_{sf}+v_y\cos\psi_{sf}}{V_t}\right)^2}} - \dot{\psi}\,\frac{\gamma}{V_t^2\sqrt{1-\left(\frac{-v_x \sin\psi_{sf}+v_y\cos\psi_{sf}}{V_t}\right)^2}} \tag{33}$$

where

$$\rho = -\dot{\psi_{sf}}\, v_x \cos\psi_{sf} - \dot{\psi_{sf}}\, v_y \sin\psi_{sf} + ||v_r||\dot{\psi}_r \cos\left(\psi_r - \psi_{sf}\right) + \dot{v}_r \sin\left(\psi_r - \psi_{sf}\right) \tag{34}$$

and

$$\gamma = \left(-w_x \sin\psi + w_y \cos\psi\right) \times (-v_x \sin\psi_{sf} + v_y \cos\psi_{sf}). \tag{35}$$

Equation 33 can be cast in the compact form

$$\dot{\bar{\psi}}_d = P - \dot{\psi}\,\Gamma \tag{36}$$

with

$$P = \frac{\rho}{V_t\sqrt{1-\left(\frac{-v_x \sin\psi_{sf}+v_y\cos\psi_{sf}}{V_t}\right)^2}} \tag{37}$$

and

$$\Gamma = \frac{\gamma}{V_t^2\sqrt{1-\left(\frac{-v_x \sin\psi_{sf}+v_y\cos\psi_{sf}}{V_t}\right)^2}}. \tag{38}$$

To derive a control law for ground target tracking, consider now the Lyapunov function

$$V_1 = \frac{1}{2}\left(y_1^2 + \frac{1}{g_2}\,\tilde{\psi}^2\right), \tag{39}$$

where $\tilde{\psi} = \bar{\psi} - \bar{\psi}_d$ and $g_2 > 0$. Differentiating V_1 with respect to time yields

$$\begin{aligned}\dot{V}_1 &= y_1\,\dot{y}_1 + \frac{1}{g_2}\,\tilde{\psi}\,\dot{\tilde{\psi}} \\ &= V_t\, y_1 \sin\tilde{\psi}\cos\bar{\psi}_d + V_t\, y_1 \cos\tilde{\psi}\sin\bar{\psi}_d \\ &\quad + y_1\left(v_x \sin\psi_{sf} - v_y\cos\psi_{sf}\right) \\ &\quad + \frac{1}{g_2}\,\tilde{\psi}\left(u_\psi - \dot{\bar{\psi}}_d\right).\end{aligned} \tag{40}$$

Since, by definition (cf. Eq. 25),

$$V_t \sin\bar{\psi}_d + v_x \sin\psi_{sf} - v_y\cos\psi_{sf} = 0 \tag{41}$$

the previous expression is equivalent to:

$$\begin{aligned}\dot{V}_1 &= V_t\, y_1 \sin\tilde{\psi}\cos\bar{\psi}_d \\ &\quad + y_1\left(v_x \sin\psi_{sf} - v_y\cos\psi_{sf}\right)\left(1-\cos\tilde{\psi}\right) \\ &\quad + \frac{1}{g_2}\,\tilde{\psi}\left(u_\psi - P + \dot{\psi}\,\Gamma\right)\end{aligned} \tag{42}$$

Fig. 5 ANTEX-M X02

Table 1 ANTEX-M X02–main features

Maximum takeoff weight	10 Kg
Wingspan	2.415 m
Payload	4 Kg
Maximum speed	100 Km/h
Autonomy	1.5 h

with $u_\psi = \dot{\psi} - \kappa\,\dot{s}$ (please refer to Eq. 21). The control law

$$\dot{\psi} = \Bigg(-g_1\,\tilde{\psi} + \kappa\,\dot{s} + P - g_2\,y_1\left(v_x\,\sin\psi_{sf} - v_y\cos\psi_{sf}\right)\frac{1-\cos\tilde{\psi}}{\tilde{\psi}} - g_2\,V_t\,y_1\,\cos\bar{\psi}_d\frac{\sin\tilde{\psi}}{\tilde{\psi}}\Bigg)/(1+\Gamma) \tag{43}$$

with $g_1, g_2 > 0$ makes

$$\dot{V}_1 = -\frac{g_1}{g_2}\tilde{\psi}^2 \leqslant 0. \tag{44}$$

Given the definition of V_1 and the fact that $\dot{V}_1 \leqslant 0$, errors $\tilde{\psi}$ and y_1 are bounded. Computing the second derivative of V_1 one can easily verify that the boundedness of the state variables implies that $\dot{V}_1$ is uniformly continuous. Hence Barbalat's lemma [21] allows for the conclusion that $\dot{V}_1$ and consequently $\tilde{\psi}$ tend to zero.

Rewritting Eq. 43 as

$$\dot{\tilde{\psi}} = -g_1\,\tilde{\psi} - g_2\,y_1\left(v_x\,\sin\psi_{sf} - v_y\cos\psi_{sf}\right)\frac{1-\cos\tilde{\psi}}{\tilde{\psi}} - g_2\,V_t\,y_1\,\cos\bar{\psi}_d\frac{\sin\tilde{\psi}}{\tilde{\psi}}, \tag{45}$$

differentiating $\dot{\tilde{\psi}}$ with respect to time, and invoking the boundedness of the variables involved, one can conclude that $\ddot{\tilde{\psi}}$ is uniformly continuous and apply once more Barbalat's lemma to conclude that $\dot{\tilde{\psi}}$ tends to zero, which leads to the conclusion that also y_1 tends to zero. The here proposed control law (Eq. 43) is the generalization of the classical path following control law [10] for paths that are moving in time. The $\dot{\psi}$ control law (Eq. 43) is converted to a bank reference for the inner-loop controller through the coordinated turn relation [22]

$$\phi = \arctan\left(\frac{\dot{\psi}\,U_0}{g}\right), \tag{46}$$

where U_0 is the aircraft's airspeed and g is the gravitational acceleration.

3 Flight Tests Results

The ground target tracking algorithm was implemented and tested on the ANTEX-M X02 platform (Fig. 5). This is one of the platforms built from scratch at AFA and available for tests within the PITVANT project. The main characteristics of ANTEX-M X02 are listed in Table 1.

The platform is equipped with a Piccolo II controller that deals with the inner control loop of the UAV. Thus, the Piccolo controls the vehicle dynamics, setting the control surface's deflections and the engine power required to follow the references provided by the ground target tracking

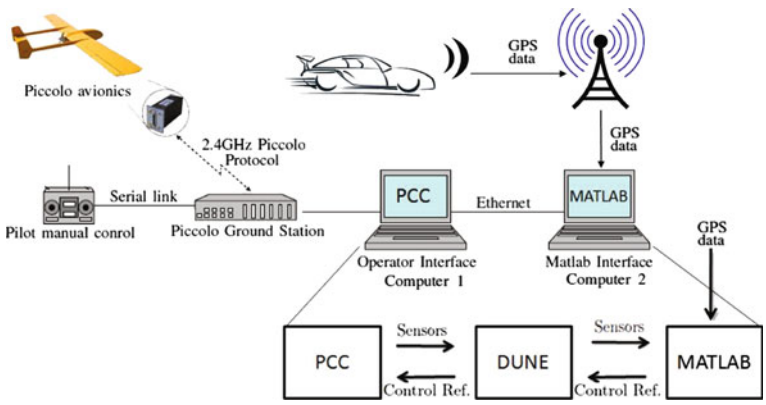

Fig. 6 Fligth test operation frame

Table 2 Controller parameters

$g_1 = 0.22$
$g_2 = 0.00007$

algorithm, given the UAV current state provided by its sensors. It relies on a mathematical model parameterized by the aircraft geometric data and has a built in wind estimator. Several model and controller parameters can be set by the user (please refer to [23]). In this work, the parameters collected from more than 30 h of flight with the ANTEX-M X02 were used.

The control algorithms for the UAV were implemented on a laptop (Computer 1) connected to the Piccolo Command Center (running on another computer–Computer 2) via an ethernet port to receive the sensor data from the Piccolo autopilot and provide the references to the aircraft (Fig. 6). The communications between these two computers is mediated by the DUNE software, developed at FEUP [24]. Computer 1 was also receiving the GPS coordinates (from a 3G GSM service) of the target and, after receiving the sensors data from the Piccolo, it computes and provides the Piccolo Command Center (Computer 2) with the control references that are then sent to the Piccolo autopilot at a telemetry rate of 1 Hz. All flight data was monitored at the base station using the Piccolo Command Center. At any time a manual pilot can take control of the aircraft providing an additional degree of safety. In future implementations, the control law will be implemented on the PC/104 onboard the aircraft and the target's position and velocity will be acquired using passive sensors onboard the aircraft.

For the field tests, a few safety measures were introduced. The bank reference sent to the aircraft was limited to 25°. The telemetry signals from the aircraft were synchronized with the GPS data of

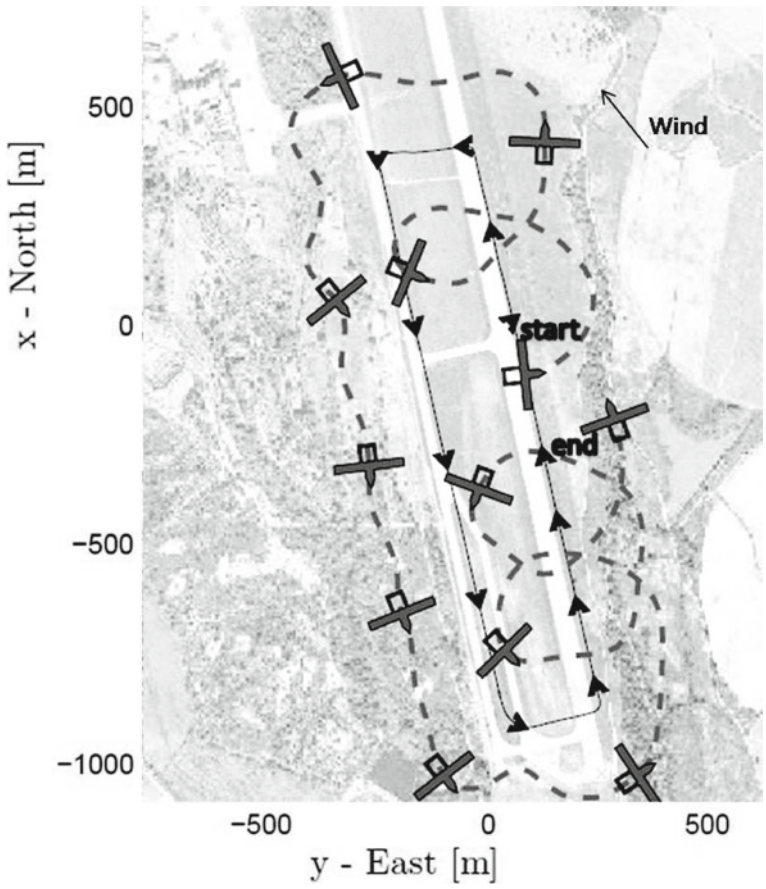

Fig. 7 Aircraft's trajectory following a target on the ground

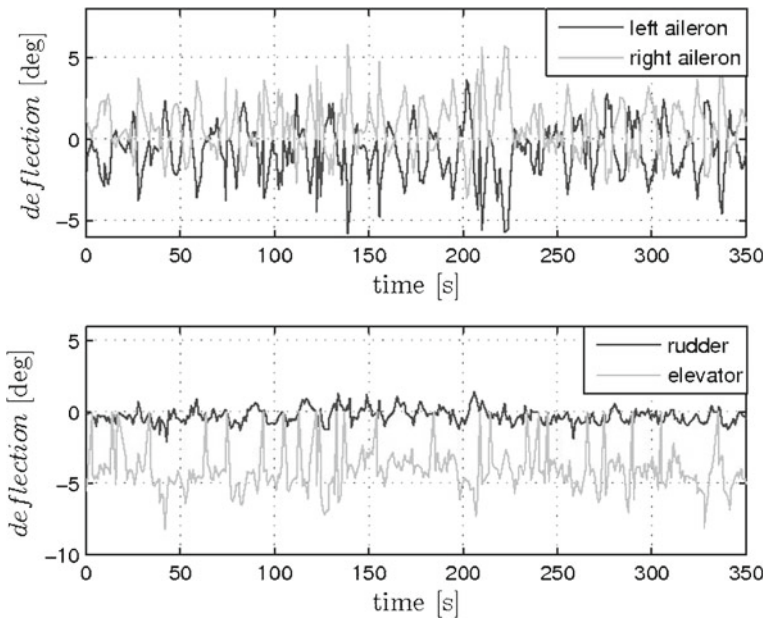

Fig. 8 Elevator, rudder and ailerons deflections

the target at 1 Hz and then fed to the controller to compute the bank reference to the aircraft. In the event of communications loss, the Piccolo assumed the last bank reference for a maximum period of 5 s. After that period, the mission would be aborted and the aircraft would be sent to the lost-comm waypoint.

In the results presentend below, the UAV was required to track a ground vehicle 200 m above the ground in the presence of moderate wind with 3 m/s average speed. An UAV airspeed of 18 m/s and a circumference radius of 200 m were chosen. The controller parameters were set to the values listed in Table 2.

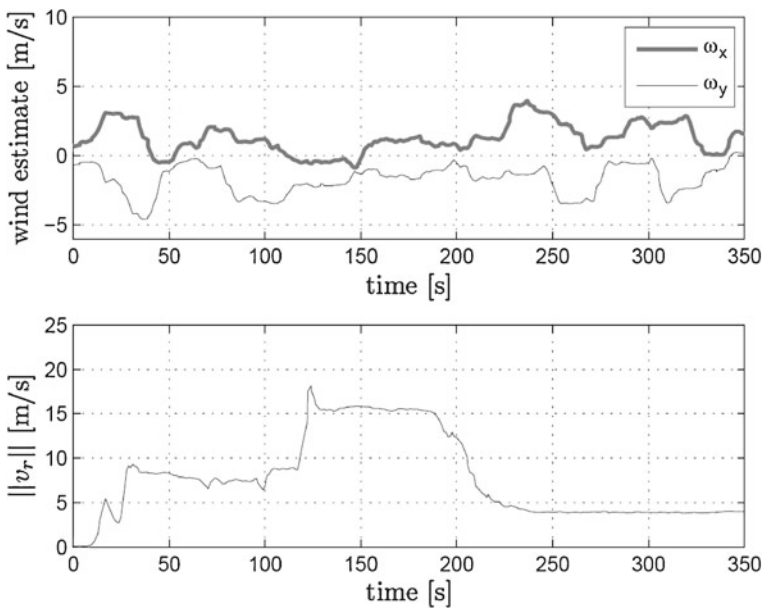

Fig. 9 Wind estimate and target's speed

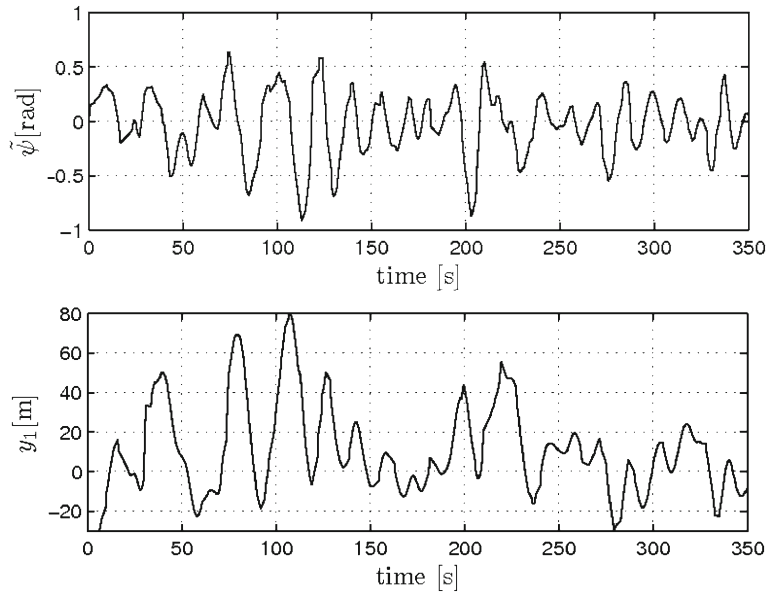

Fig. 10 Position and heading errors

Figure 7 shows the overall vehicle trajectory and from Fig. 8 one can see that the control surface deflections are kept within their linear regions. Figure 9 shows the target's speed and the wind estimate. The target starts moving North (starting close to the origin of the local inertial frame (Fig. 7) at 8 m/s and then turns West, keeping its speed. The UAV loiters above it. When the target reaches the Northwest top of its journey, it starts to head South at 15 m/s, almost reaching the aircraft's ground speed. In this situation, Fig. 7 shows that the path following control law requires the UAV to move in a straight line in the same direction of the target. After reaching the top South of its path, the target slows down to 4 m/s and turns back to head North. Now, the aircraft starts again to loiter around the target until it returns close to its place of departure.

Distance and angular errors are depicted in Fig. 10 showing the good performance of the control strategy, even in the presence of relatively large communication latency (Fig. 11). Comunications losses will be greatly reduced (improving system performance) when the control law is implemented onboard the aircraft (with direct access to the sensors data). Figure 12 shows that the bank reference sent to the aircraft was saturated for small periods of time, thus decreasing the system's performance. However, the control system proved to be sufficiently robust, tackling all these situations that were not taken into account during control design.

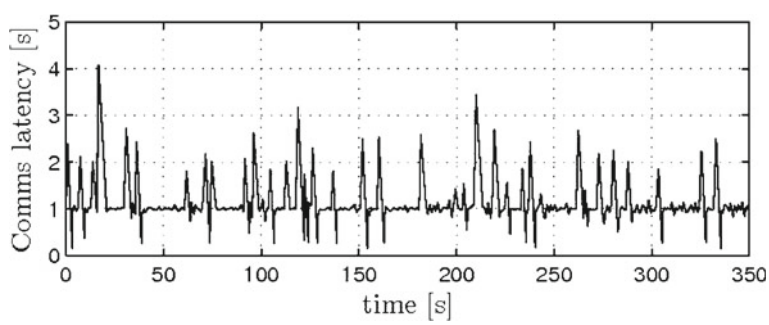

Fig. 11 Communications latency

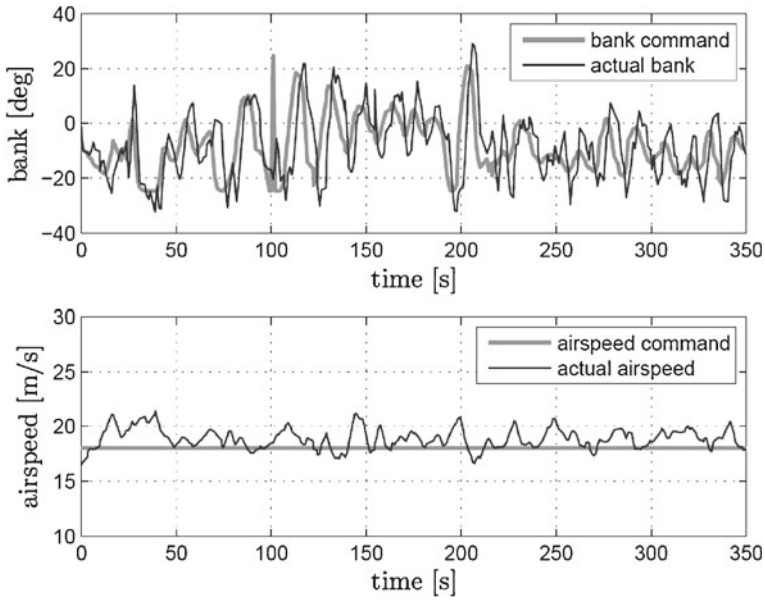

Fig. 12 Airspeed and bank reference commands and real values

4 Conclusions

A control law for ground target tracking was presented. The control law was derived at the kinematic level, relying on an onboard controller to control the vehicle dynamics. Formal convergence proofs are provided for the kinematic controller along with flight test results with the ANTEX-X02 aircraft which demonstrate how well the overall system performs. Future work will include the implementation of the control laws in the PC104 onboard the aircraft and will address the problem of acquiring the target position and velocity using passive sensors onboard the aircraft (e.g. video camera). Additionally, the control system will be analysed from the control surface deflections profile perspective. Optimization strategies in order to minimize energy expenditure and control surfaces wear and tear will be sought.

Acknowledgements The authors would like to acknowledge the contribution of Second Lieutenant Gonçalo Cruz from the Portuguese Air Force Academy. The authors are also in debt to every member of the PITVANT research team.

References

1. Lee, J., Huang, R., Vaughn, A., Xiao, X., Hedrick, K., Zennaro, M., Sengupta, R.: Strategies of path-planning for a UAV to track a ground vehicle. In: Proceedings of the 2nd Annual Autonomous Intelligent Networks and Systems Conference (2003)
2. Spry, S., Vaughn, A., Xiao, X.: A vehicle following methodology for UAV formations. In: Proceedings of the 4th International Conference on Cooperative Control and Optimization (2003)
3. Dobrokhodov, O., Kaminer, I., Jones, K., Ghabcheloo, R.: Vision-based tracking and motion estimation for moving targets using small UAVs. In: Proceedings of the AIAA Guidance Navigation and Control Conference and Exibit (2006)
4. Li, Z., Hovakimyan, N., Dobrokhodov, V., Kaminer, I.: Vision-based target tracking and motion estimation using a small UAV. In: Proceedings of the 49th IEEE Conference on Decision and Control, pp. 2505–2510 (2010)
5. Frew, E., Lawrence, D., Dixon, C., Elston, J., Pisano, J.: Lyapunov guidance vector fields for unmanned aircraft applications. In: Proceedings of the 2007 American Control Conference, pp. 371–376 (2007)
6. Samson, C.: Path following and time-varying feedback stabilization of wheeled mobile robots. In: Proceedings of the International Conference on Advanced Robotics and Computer Vision, vol. 13 (1992)
7. Micaelli, A., Samson, C.: Trajectory tracking for unicycle-type and two-steering-wheels mobile robots. INRIA, Tech. Rep. (1993)
8. Canudas de Wit, C., Khennouf, H., Samson, C., Sordalen, O.J.: Nonlinear control design for mobile robots. In: Zheng, Y. (ed.) Recent Trends in Mobile Robots. World Scientific Series in Robotics and Automated Systems, vol. 11, pp. 121–156. World Scientific (1993)
9. Ren, W., Beard, R.: Trajectory tracking for unmanned air vehicles with velocity and heading rate constraints. IEEE Trans. Control Syst. Technol. **12**, 706–716 (2004)

10. Encarnação, P., Pascoal, A., Arcak, M.: Path following for marine vehicles in the presence of unknown currents. In: Proceedings of SYROCO 2000-6th International IFAC Symposium on Robot Control, pp. 469–474 (2000)
11. Encarnação, P., Pascoal, A.: 3D path following for autonomous underwater vehicles. In: Proceedings of the 39th Conference on Decision and Control, pp. 2977–2982 (2000)
12. Lapierre, L., Soetanto, D., Pascoal, A.: Adaptive, non-singular path-following control of dynamic wheeled robots. In: Proceedings of the 42nd IEEE Conference on Decision and Control, vol. 2, pp. 1765–1770 (2003)
13. Kaminer, I., Yakimenko, O., Dobrokhodov, V., Pascoal, A., Hovakimyan, N., Cao, C., Young, A., Patel, V.: Coordinated path following for time-critical missions of multiple UAVs via L1 adaptive output feedback controllers. In: Proceedings of the AIAA Guidance, Navigation and Control Conference (2008)
14. Kaminer, I., Yakimenko, O., Pascoal, A., Ghabcheloo, R.: Path generation, path following and coordinated control for time-critical missions of multiple UAVs. In: Proceedings of the 2006 American Control Conference, pp. 4906–4913 (2006)
15. Wise, R., Rysdyk, R.: UAV coordination for autonomous target tracking. In: Proceedings of the AIAA Guidance, Navigation, and Control Conference and Exhibit (2006)
16. Oliveira, T., Encarnação, P.: Ground target tracking for unmanned aerial vehicles. In: Proceedings of the AIAA Guidance, Navigation, and Control Conference (2010)
17. Aguiar, A., Kaminer, I., Ghabcheloo, R., Pascoal, A., Xargay, E., Hovakimyan, N., Cao, C., Dobrokhodov, V.: Time-coordinated path following of multiple UAVs over time-varying networks using L1 adaptation. In: Proceedings of the AIAA Guidance, Navigation and Control Conference and Exhibit (2008)
18. Kaminer, I., Howard, R.: Avionics technology development for CR and VTOL UAV. Naval Post Graduate School, Tech. Rep. (1993)
19. Bishop, L.: There is more than one way to frame a curve. Am. Math. Mon. **82**, 246–251 (1975)
20. Craig, J.: Introduction to Robotics: Mechanics and Control. Addison-Wesley, New York (1986)
21. Khalil, H.: Nonlinear Systems. Prentice Hall (2002)
22. Donald, M.: Automatic Flight Control Systems. Prentice Hall (1990)
23. Piccolo Hardware-in-Loop/Software-in-Loop Setup Guide: Cloud Cap Technology (2008)
24. Martins, R., Dias, P., Marques, E., Pinto, J., Sousa, J., Pereira, F.: IMC: a communication protocol for networked vehicles and sensors. In: Proceedings of the IEEE Oceans Europe'09, pp. 1–6 (2009)